Sharp quantum phase transition in the frustrated spin-1/2 Ising chain antiferromagnet CaCoV$_2$O$_7$

Isha [1], A. K. Bera,[2,3,*] Guratinder Kaur,[4,5] C. Stock,[5] Koushik Chakraborty,[1] Pascal Puphal,[4] M. Isobe,[4]
K. Küster,[4] Y. Skourski,[6] L. Bhaskaran [6] S. A. Zvyagin,[6] S. Luther,[6,7] J. Gronemann,[6] H. Kühne,[6]
C. Salazar Mejía,[6] M. Pregelj [8] Thomas C. Hansen [9] S. D. Kaushik,[10] David Voneshen,[11,12] R. Kulkarni,[13]
N. P. Lalla,[1] S. M. Yusuf [2,3] A. Thamizhavel [13] and Arvind Kumar Yogi [1,13,†]

[1]*UGC-DAE Consortium for Scientific Research*, Indore-452001, India
[2]*Solid State Physics Division, Bhabha Atomic Research Centre, Mumbai 400085, India*
[3]*Homi Bhabha National Institute, Anushaktinagar, Mumbai 400094, India*
[4]*Max-Planck-Institut für Festkörperforschung, Heisenbergstr. 1, D-70569 Stuttgart, Germany*
[5]*School of Physics and Astronomy, University of Edinburgh, Edinburgh EH9 3JZ, United Kingdom*
[6]*Dresden High Magnetic Field Laboratory (HLD-EMFL), Helmholtz-Zentrum Dresden-Rossendorf, 01328 Dresden, Germany*
[7]*Institut für Festkörper- und Materialphysik, TU Dresden, 01062 Dresden, Germany*
[8]*Jožef Stefan Institute, Jamova c. 39, SI-1000 Ljubljana, Slovenia*
[9]*Institut Max von Laue-Paul Langevin, 71 avenue des Martyrs, 38042 Grenoble, France*
[10]*UGC-DAE Consortium for Scientific Research, Mumbai Centre 246-C CFB, BARC, Mumbai 400085, India*
[11]*SIS Facility, STFC Rutherford Appleton Laboratory, Harwell Oxford, Didcot OX11 0QX, United Kingdom*
[12]*Department of Physics, Royal Holloway University of London, Egham TW20 0EX, United Kingdom*
[13]*Department of Condensed Matter Physics and Materials Science, Tata Institute of Fundamental Research,*
Homi Bhabha Road, Colaba, Mumbai 400 005, India

We report on a quantum critical behavior in the quasi-1D spin-1/2 zigzag frustrated chain antiferromagnet CaCoV$_2$O$_7$, induced by an applied magnetic field. Below $T_N = 3.3$ K our zero-field neutron diffraction studies revealed the up-up-down-down spin structure, stabilized by an order-by-disorder phenomenon. At base temperature, the magnetic order is suppressed by an applied magnetic field (B), inducing a transition into a quantum paramagnetic state at $B_c = 3$ T, as revealed by both neutron diffraction and ESR data. The transition exhibits an unusually sharp phase boundary with the critical exponent $\phi = 0.164(3) \approx 1/6$, in contrast to the earlier experimental observations for uniform spin-1/2 chain systems. Such a sharp QPT is anticipated due to a rare combination of spin-orbit coupling and competing NN and NNN exchange interactions J_1 and J_2 of the zigzag spin chain.

A quantum phase transition (QPT) occurs at zero temperature and is controlled by a nonthermal parameter such as pressure, chemical substitution, magnetic field, etc. The associated quantum critical fluctuations driven by the Heisenberg uncertainty principle often give rise to exotic behavior that is in a sharp contrast to the conventional temperature induced phase transition [1–4]. At zero temperature, QPT is continuous through a quantum critical point (QCP) which extends to a broad V-shaped region of quantum criticality at a nonzero temperature, where the physical properties show universal features, which are independent of microscopic details. The criticalities around QCP may reflect inherent quantum dynamics of the system as quantum critical

fluctuations in the vicinity of QPTs and reveal unusual universality classes, demonstrating numerous exotic phenomena such as unconventional superconductivity [5,6], quantum E8-symmetry integrable system [7], many-body string excitations [8,9], novel quantum criticality [10–15] in transverse field Ising chains, and Bose-Einstein condensation (BEC) [16].

The exactly solvable model spin systems, in particular, 1D spin-chain systems, often provide an opportunity to explore the QPTs and quantum criticality [2,17]. One important model is the spin-1/2 XXZ chain

$$H = J \sum_i \left[\left(\tilde{S}_i^z \tilde{S}_{i+1}^z \right) + \epsilon \left(\tilde{S}_i^x \tilde{S}_{i+1}^x + \tilde{S}_i^y \tilde{S}_{i+1}^y \right) + g\mu_B \vec{B}.\vec{S}_i \right],$$

where $\vec{S}_i$ is the spin-1/2 operator on the ith site, g is the electronic g factor, μ_B is the Bohr magneton, and $0 < \epsilon < 1$ takes into account the Ising-like anisotropy of magnetic interaction. For this model, a field induced QPT is predicted with a critical exponent $\phi = 0.5$ or 1 [$T_N \propto (B_c - B)^\phi$] for the 3D or 1D QCP which are experimentally realized in the 1D uniform spin-chain materials CoNb$_2$O$_6$ [7] and (Sr/Ba)Co$_2$V$_2$O$_8$ [18,19] with ferromagnetic and antiferromagnetic (AFM) ground states, respectively.

*Contact author: akbera@barc.gov.in
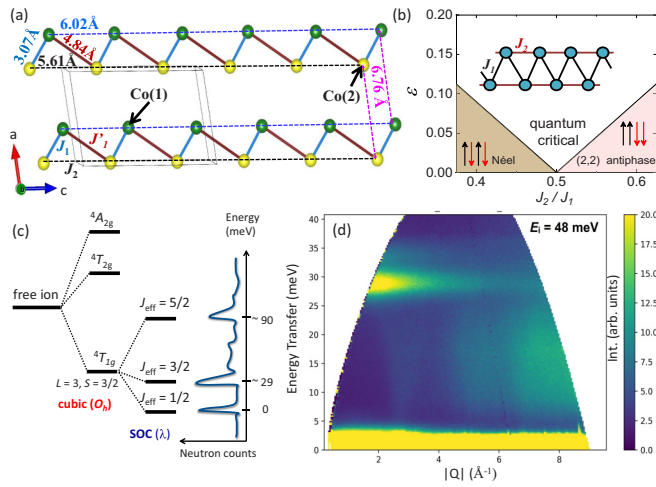†Contact author: akyogi@csr.res.in

FIG. 1. (a) A Schematic representation of the zigzag spin-chain in $CaCoV_2O_7$. The possible exchange interactions and the corresponding direct distances between magnetic Co^{2+} ions are shown. The green and yellow solid circles are the Co atoms at two different Wyckoff sites. (b) The ground-state phase diagram for a zigzag spin-1/2 chain [21], with the NN: J_1, NNN: J_2 intrachain interactions and the anisotropy parameter ϵ. The inset shows a model/ideal zigzag chain with J_1 and J_2 interactions. (c) The Inelastic neutron scattering spectrum of $CaCoV_2O_7$ revealing the CFE at ≈ 29.5 meV, as expected from the (d) CFE energy levels of the Co^{2+} ions in an octahedral environment, resulting in a pseudospin-1/2 ground state doublet.

We report here an unusually sharp QPT with a critical exponent $\phi = 0.164(3)$ in the spin-1/2 zigzag AFM chain compound $CaCoV_2O_7$ with competing intrachain nearest-neighbor (NN: J_1) and next-nearest-neighbor (NNN: J_2) exchange interactions [Fig. 1(a)]. In general, the 1D zigzag spin-1/2 chain model, comprising of competing intrachain J_1 and J_2 exchange interactions [Fig. 1(a)], are of particular interest due to numerous field-induced quantum phenomena [20], induced by a combined effect of the geometrical spin frustration and quantum fluctuations [21,22]. In the Ising limit this theoretical model yields an up-down-up-down (UDUD: Néel) phase and an up-up-down-down (UUDD: double Néel) phase as a function of J_2/J_1 and the phases are separated by a QCP at $J_2/J_1 = 0.5$ [Fig. 1(b)]. Such ordered magnetic ground states are fragile and can be suppressed by an external magnetic field, leading to a field-induced QPT to novel quantum spin states [21,22]. In this Letter, we show that the spin-1/2 zigzag AFM chain compound $CaCoV_2O_7$ hosts an UUDD AFM ground state, implying that $J_2/J_1 \geqslant 0.5$ [21]. We further show that such a UUDD AFM ground state can be suppressed by a reasonably low applied magnetic field of $B_c \sim 3$ Tesla (QCP), leading to an order-to-disorder QPT.

The polycrystalline samples of $CaCoV_2O_7$ and it's non-magnetic analog $CaMgV_2O_7$ were prepared by a solid state reaction method described in Ref. [23]. First single-crystalline samples of $CaCoV_2O_7$ were grown using an optical floating zone furnace (Crystal System Co., Japan). The temperature and magnetic field dependent magnetization measurements were performed by using SQUID magnetometer (Quantum Design). The heat capacity $C_p(T)$ measurements were

performed using a commercial physical property measurement system (PPMS, Quantum Design). The electron spin resonance (ESR) spectra were performed employing a 16 T transmission-type multifrequency ESR spectrometer similar to that described in Ref. [24], and fitting was performed using easyspin simulation [25]. High-field magnetization was measured at the HLD, Dresden, Germany, using a pulsed magnet with a rise time of 7 ms and a total pulse duration of 25 ms. The magnetization was obtained by integrating the voltage induced in a compensated coil system surrounding the sample [26]. X-ray photoelectron spectra (XPS) were acquired with a Kratos Axis Ultra system (Manchester) using a monochromatized Al K_α (1486.6 eV) source. The zero-field neutron diffraction patterns were recorded at two different wavelengths (λ) 1.54 Å and 2.41 Å by using the D20 powder diffractometer at the Institut Laue-Langevin (ILL), Grenoble, France. Magnetic field dependent neutron diffraction patterns were recorded at 2 K using the powder diffractometer PD-3 (λ) 1.48 Å, Dhruva Reactor, BARC, Mumbai [27]. The measured diffraction patterns [Fig. 3(b)] were analyzed by using the Rietveld refinement technique implemented in the Fullprof suite program [28]. $CaCoV_2O_7$ is regarded as a model spin-1/2 XXZ zigzag spin chain compound. The zigzag spin chains of Co^{2+} [Fig. 1(a)] in $CaCoV_2O_7$ are made up of corner-sharing CoO_6 octahedra, VO_5 pyramids, and VO_4 tetrahedra along the crystallographic c axis [for details see the Supplemental Material (SM) Note I [29] and Fig. S2] leading to nearest-neighbour (J_1 and J_1') and next-nearest-neighbour J_2 exchange interactions. Our inelastic neutron scattering spectra clearly reveals a crystal field excitation level at around 29.5 meV, confirming the presence of a spin-orbit coupled pseudo-spin-1/2 ground state in $CaCoV_2O_7$ with a pronounced Ising anisotropy [7,8,30–34] (for details see Notes VI and VII in the SM [29]). The magnetic easy axis is along the c axis, as reflected by isothermal magnetization curves measured on a single crystal [Fig. 2(c)], as well as anisotropic g factors $g_\parallel/g_\perp \sim 2$ (see ESR results below).

The temperature dependent susceptibility and specific heat curves of $CaCoV_2O_7$ reveal anomalies at $T_N = 3.3$ K [Fig. 2(a)], indicating the onset of a long-range AFM ordering. Further, both the susceptibility and magnetic heat-capacity curves show a broad hump centered around $\sim$6 K indicating the presence of short-range magnetic ordering [35]. The temperature dependent susceptibility curve of $CaCoV_2O_7$, is well accounted by an AFM spin-1/2 chain model (Bonner-Fisher model [33]) with an exchange coupling of $\sim$4.8 K and the g value of 5.8 [Fig. 2(b)]. Furthermore, the derived magnetic entropy S_{mag} value of 6.8 J/mol K, obtained by integration of $C_{mag}(T)/T$ curve up to 80 K, is reasonably close to the value $S_{mag} = R \ln 2 = 5.76$ J/mol K, as expected for a spin-1/2 system [see Note II in the SM [29] and Fig. S5(b)] [36].

Single crystal study reveals that the QPT occurs only for the longitudinal field, i.e., along the c direction (easy axis) [Fig. 2(c)]. The field dependent magnetization (M) curves measured at 1.4 K [Fig. 2(c) and Fig. S7(d) [29]] reveals the field-induced transition at $\sim$3 T and at higher-fields it shows an asymptotic approach of saturation [Fig. S7(d) [29]] [37]. This transition at $\sim$3 T is characterized as a QPT by the field dependent heat capacity [Fig. 2(d)] and magnetic-susceptibility [Fig. S7(d) [29]] study. Further, it has been
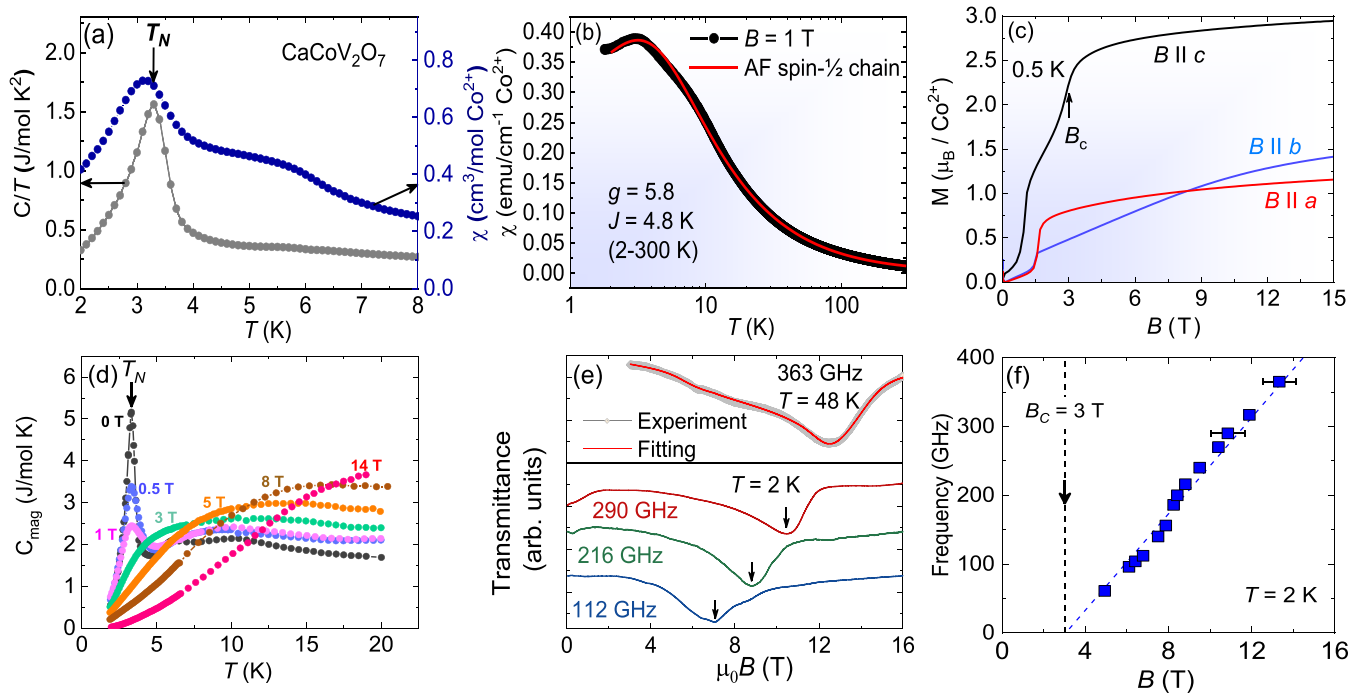
FIG. 2. (a) The temperature dependent magnetic susceptibility χ at 0.1 T and zero field specific heat C curves of CaCoV$_2$O$_7$ over low temperatures below 8 K. (b) The $\chi(T)$ curve at 1 T and the fitted curve (solid line) by an AFM spin-1/2 chain model (Bonner-Fisher model [33]). (c) Pulsed-field magnetization of a single-crystalline CaCoV$_2$O$_7$ sample for fields applied along the crystallographic main axes. The low field transitions at 1 T for $B \parallel c$ and 1.5 T for $B \parallel a$ and b are due to the field induced phase transition of the secondary phase. All magnetization data are scaled in μ_B and normalized to the value at 15 T, yielding anisotropic and pronounced slope changes of the field-dependent sample magnetization. (d) The magnetic specific heat (C_{mag}) curve of CaCoV$_2$O$_7$ after subtraction of the lattice contribution estimated by the measured curve for CaMgV$_2$O$_7$. (e) ESR spectrum taken at a temperature of 48 K and a frequency of 363 GHz is shown in light gray. The fit was made for powder ESR spectrum using the effective spin Hamiltonian as determined in the text with the best fit parameters $g'_x = 1.85$, $g'_y = 2.17$, and $g'_z = 5.35$ is shown by the red solid line. Examples of ESR spectra at a temperature of 2 K and frequencies of 290 GHz, 216 GHz, and 112 GHz are shown in brown, green, and purple, respectively (the spectra are normalized by the zero-field transmittance background and offset for clarity). (f) Frequency-field diagram of magnetic excitations in CaCoV$_2$O$_7$ at 2 K (positions of absorption maxima are shown). Lines are guides to the eye.

confirmed that there is no hysteresis in the $M\,vs\,B$ data across the QPT [Fig. 2(c) and Fig. S7(d) [29]].

The ESR spectrum measured at 48 K with a frequency of 363 GHz shows a distinct resonance spanning over a wide magnetic field range [Fig. 2(e)], which is typical for octahedral high-spin Co^{2+} powder species [38]. The recorded spectrum has been analyzed employing the following effective spin-Hamiltonian: $H = \mu_B \mathbf{B} g' \tilde{S}$, where **B** is the external magnetic field, g' is the effective g tensor, $\tilde{S}$ is the pseudospin $= 1/2$ operator, and μ_B is the Bohr magneton. A best fit of the experimental spectrum [Fig. 2(e)] was obtained for $g'_x = 1.85$, $g'_y = 2.17$, and $g'_z = 5.35$. The anisotropic g' values, originating from the trigonally distorted CoO$_6$ octahedral crystal field, confirm the Ising nature of CaCoV$_2$O$_7$ with an easy axis along the c axis. The low energy ESR spectra [Fig. 2(f)], measured at 2 K, reveals an appearance of a linear frequency-field dependence mode above the $B_c = 3$ T. This mode persists at temperatures well above T_N (it was observed at least up to 50 K) and it appears to be characteristics of the field-induced quantum disordered state. The observed mode is reminiscent of the psinon-antipsinon pair excitations reported for the 1D Heisenberg-Ising antiferromagnet SrCo$_2$V$_2$O$_8$ [8,9], strongly

motivating us for future ESR studies of magnetic excitations in single-crystal CaCoV$_2$O$_7$ samples.

The magnetic ground state of CaCoV$_2$O$_7$ has been investigated by powder neutron diffraction. Figure 3(a) gives an overview of the neutron diffraction data recorded at different temperatures below and above $T_N = 3.3$ K. With decreasing temperature, a broad diffuse magnetic peak appears at $Q \approx 0.67\,\text{Å}^{-1}$, below $\sim$6 K, and reveals the presence of short-range magnetic correlations (in agreement with the susceptibility and heat capacity curves), a characteristic feature of a 1D spin system [39]. With further decreasing temperature, the broad peak becomes more intense and sharper, and it transforms into the magnetic Bragg peak below $T_N = 3.3$ K of the long-range 3D magnetic order state.

All the magnetic peaks corresponding to CaCoV$_2$O$_7$ can be indexed with the propagation vector $\mathbf{k} = (\frac{1}{2}\ 0\ 0)$. The magnetic structures compatible with **k** and the crystal symmetry are analyzed with the representation analysis using the BASIREPS program available in the Fullprof suite [28]. The symmetry analysis reveals that there are four possible magnetic structures corresponding to the four nonzero irreducible representations (IRs) Γ_ν. The magnetic reducible
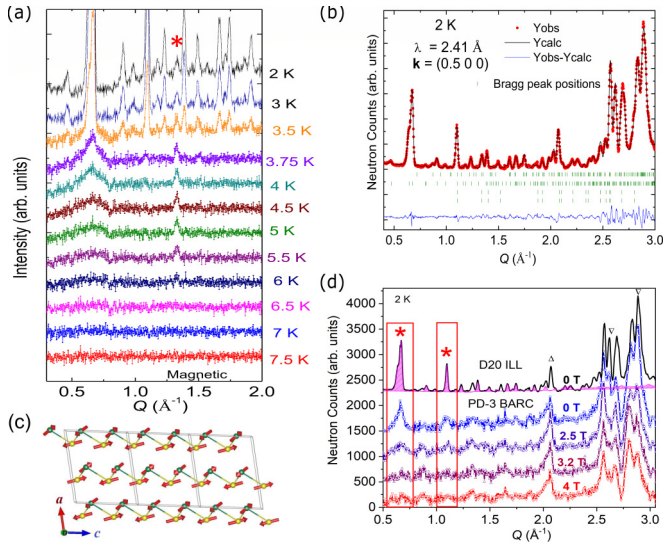
FIG. 3. (a) The temperature dependence of the magnetic neutron diffraction patterns of $CaCoV_2O_7$ over the temperatures 2–7.5 K, after the subtraction of nuclear background at 8 K. The additional Bragg peak at $Q \sim 1.4$ Å^{-1} (marked by asterisks) is from the magnetic phase of $Co_3V_2O_8$. (b) Experimentally observed (red circles) and calculated (black solid lines) neutron diffraction pattern for the four phase model (nuclear and magnetic phases for $CaCoV_2O_7$ and $Co_3V_2O_8$) at 2 K. The difference between observed and calculated patterns is shown by the thin blue line at the bottom. The vertical bars are the theoretical Bragg peak positions for nuclear and magnetic phases. (c) A schematic of the UUDD magnetic structure for $CaCoV_2O_7$. (d) Field evolution of the neutron diffraction patterns at 2 K. Intensity of the magnetic peaks were fully suppressed above 3 T as shown by red stars. The zero field neutron diffraction pattern measured by using the D20 diffractometer, ILL, [as shown in the right panel of Fig. 3(b)] is also included for a reference. The up and down triangles represent the nuclear Bragg peaks which have changes in the intensities with the magnetic field due to a reorientation of the powder samples under applied magnetic field.

representation Γ_{mag} for both the magnetic sites is composed of four IRs as $\Gamma_{Mag}^{Co(1),Co(2)} = 3\Gamma_1^1 + 3\Gamma_2^1 + 3\Gamma_3^1 + 3\Gamma_4^1$.

The basis vectors of these IRs for the two sites Co(1) and Co(2) are given in Table S6 of the SM [29]. Out of the four possible magnetic structures, i.e., four Γs, the best refinement of the experimental magnetic diffraction pattern is obtained for Γ_4 (Fig. 3). The corresponding magnetic structure for $CaCoV_2O_7$ is shown in Fig. 3(c). Thus, the magnetic structure is composed of an UUDD spin arrangement along the chain, as predicted for an Ising J_1-J_2 zigzag AFM chain in the high frustration regime with $J_2/J_1 \geqslant 0.5$ (Fig. 1). The UUDD AFM ground state appears due to the order-by-disorder phenomenon, anticipated for the highly frustrated conditions $J_2/J_1 \geqslant 0.5$ within this model. Moreover, the neutron diffraction measurements under magnetic field up to 4 T at 2 K unambiguously yield the disappearance of the antiferromagnetic Bragg-peaks above $B_c = 3$ T, confirming a QPT from the AFM state to the quantum paramagnetic state [Figs. 3(d) and 2(f)].

The magnetic phase diagram [Figs. 4(a) and 4(b)] of $CaCoV_2O_7$ in the B-T plane has been determined from the
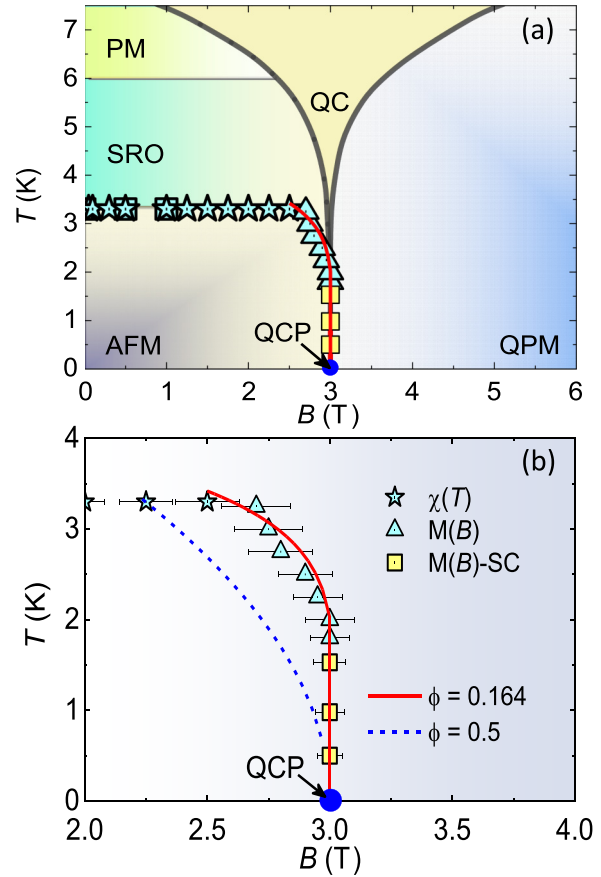

FIG. 4. (a) The magnetic phase diagram with paramagnetic (PM), antiferromagnetic (AFM), quantum-paramagnetic (QPM), and quantum critical (QC) phases. The solid red line is the calculated curve by the power law $T_N \propto (B_c - B)^\phi$. The open centered squares, stars, vertical triangles, and yellow filled squares represent the $C_p(T)$, $\chi(T)$, $M(B)$, and single-crystal $M(B)$, respectively. (b) The zoomed view of the $T(B)$ phase boundary close to the QCP. The solid red and dashed blue curves are the theoretical curves with the critical exponents $\phi = 0.164$ and 0.5, respectively.

anomalies in the $\chi(T)$ and $C_p(T)$ curves measured under several applied fields, as well as from $M(B)$ curves measured at several temperatures (for details see Note III in the SM [29]). It may be noted that the order-disorder phase boundary is very sharp close to the B_c, which makes $CaCoV_2O_7$ unique among the compounds showing magnetic-field induced QPT [40]. The power law $T_N = A(B_c - B)^\phi$ fitting of the phase boundary reveals the exponent ϕ is 0.164(3) and critical field $B_c = 3.02(4)$ T. Power-law behavior of the phase boundary is a characteristic feature of quantum criticality. Further, the magnetic Grüneisen parameter Γ_B curve [for details see Fig. S7(e) in the SM [29]] clearly distinguishes two regions viz., a quantum paramagnet where the $\Gamma_B B = 0.006$ is a constant (temperature independent) and the QC state where the $\Gamma_B B$ follows a scaling behavior with the crossover point at ~ 1.5 K/T$^{4/3}$. The order-disorder QPT is further characterized by the $\Gamma_B B$ vs B plot [inset Fig. S7(e) in the SM [29]] which shows a sign change at around the QCP, in line with the theory [41].

Our experimental results, including an UUDD AFM ground state, temperature dependent susceptibility, magnetic specific heat, and ESR, reveal that $CaCoV_2O_7$ can be well described by a highly frustrated Ising spin-1/2 zigzag J_1-J_2 AFM chain. Furthermore, our finding of a magnetic-field-induced QPT in $CaCoV_2O_7$ through a QCP at a modest magnetic field of 3 Tesla is unique as it shows an exceptionally sharp phase transition with a critical exponent $\phi = 0.164(3)$. Experimentally, QPT and quantum criticality are realized on the Ising spin chain materials $Sr/BaCo_2V_2O_8$ [18,19] and $YbAlO_3$ with AFM ground states [42], as well as $CoNb_2O_6$ [7] with FM ground state. It is reported for Ising spin-chains under transverse magnetic field that the 1D and 3D QCPs can be decoupled with the location of the 1D QCP both inside and outside of the 3D magnetically ordered phase [19,43]. For the 3D QCP, the $T(B)$ phase boundary is reported to follow a power law behavior with a mean-field-like exponent $\phi = 1/2$ [3,19]. For the 1D QCP, the $T(B)$ curve is reported to follow a straight line with the critical exponent $\phi = 1$ [18,19] in accordance with the theory [3]. On the other hand, the exponent value for the 3D QCP of the Ising spin-chain systems under a longitudinal magnetic field is reported to be $\phi = 2/3$ [44]. For the present compound $CaCoV_2O_7$, the experimentally determined value of $\phi = 0.164(3) \approx 1/6$ is significantly smaller than the values for both the transverse and longitudinal field QPTs, and hence, reveals an unusual sharp QPT.

The observed sharp QPT as found in $CaCoV_2O_7$ is rare for any condensed-matter system. We mention here that a low value of critical exponent $\phi = 0.21$ was also recently reported for $TmVO_4$ [14]. It was argued that the bilinear coupling of the nematic order parameter to acoustic phonons changes the spatial and temporal fluctuations of the former in a fundamental way, resulting in the experimentally observed low value of the critical exponent of the field induced QPT. In the present study, thus, the observation of the low value of critical exponent indicates that a rare combination of spin-orbit coupling, competing NN and NNN exchange interactions, single-ion anisotropy, and low dimensionality in $CaCoV_2O_7$ plays an important role in shaping the magnetic phase diagram. Our results motivate further investigation of the characteristic spin and lattice dynamics and their coupling in magnetic fields by Raman spectroscopic measurements or single crystal inelastic neutron scattering over full Brillouin zone.

In summary, our experimental results confirm an uncommon field-induced QPT from an ordered AFM state to a QPM state through a QCP at a moderate magnetic field of $B_c = 3$ T in the 1D zigzag Ising spin-1/2 chain antiferromagnet $CaCoV_2O_7$. The observed unusually sharp QPT with the exceptionally small critical exponent $\phi \approx 1/6$ and demands a detailed theoretical investigation. Our results also demonstrate distinctive quantum critical behaviors at the QCP, including scaling behaviors of spin dynamics by using the magnetic Grüneisen ratio.

---

[1] L. D. Landau, On the theory of phase transitions, Phys. Z. Sowjetunion **11**, 26 (1937).

[2] T. Giamarchi, *Quantum Physics in One Dimension* (Oxford University Press, Oxford, 2004).

[3] S. Sachdev, *Quantum Phase Transitions* (Cambridge University Press, Cambridge, 2011).

[4] S. L. Sondhi, S. M. Girvin, J. P. Carini, and D. Shahar, Continuous quantum phase transitions, Rev. Mod. Phys. **69**, 315 (1997).

[5] D. C. Johnston, The puzzle of high temperature superconductivity in layered iron pnictides and chalcogenides, Adv. Phys. **59**, 803 (2010).

[6] B. Keimer, S. A. Kivelson, M. R. Norman, S. Uchida, and J. Zaanen, From quantum matter to high-temperature superconductivity in copper oxides, Nature (London) **518**, 179 (2015).

[7] R. Coldea, D. A. Tennant, E. M. Wheeler, E. Wawrzynska, D. Prabhakaran, M. Telling, K. Habicht, P. Smeibidl, and K. Kiefer, Quantum criticality in an Ising chain: Experimental evidence for emergent E-8 symmetry, Science **327**, 177 (2010).

[8] Z. Wang, J. Wu, W. Yang, A. K. Bera, D. Kamenskyi, A. T. M. N. Islam, S. Xu, J. M. Law, B. Lake, C. Wu, and A. Loidl, Experimental observation of Bethe strings, Nature (London) **554**, 219 (2018).

[9] A. K. Bera, J. Wu, W. Yang, R. Bewley, M. Boehm, J. Xu, M. Bartkowiak, O. Prokhnenko, B. Klemke, A. T. M. N. Islam, J. M. Law, Z. Wang, and B. Lake, Dispersions of many-body Bethe strings, Nat. Phys. **16**, 625 (2020).

[10] Q. Faure, S. Takayoshi, S. Petit, V. Simonet, S. Raymond, L.-P. Regnault, M. Boehm, J. S. White, M. Månsson, C. Rüegg, P. Lejay, B. Canals, T. Lorenz, S. C. Furuya, T. Giamarchi, and B. Grenier, Topological quantum phase transition in the Ising-like antiferromagnetic spin chain $BaCo_2V_2O_8$, Nat. Phys. **14**, 716 (2018).

[11] S. Horiuchi, Y. Okimoto, R. Kumai, and Y. Tokura, Quantum phase transition in organic charge-transfer complexes, Science **299**, 229 (2003).

[12] T. Hong, T. Ying, Q. Huang, S. E. Dissanayake, Y. Qiu, M. M. Turnbull, A. A. Podlesnyak, Y. Wu, H. Cao, Y. Liu, I. Umehara, J. Gouchi, Y. Uwatoko, M. Matsuda, D. A. Tennant, G.-W. Chern, K. P. Schmidt, and S. Wessel, Evidence for pressure induced unconventional quantum criticality in the coupled spin ladder antiferromagnet $C_9H_{18}N_2CuBr_4$, Nat. Commun. **13**, 3073 (2022).

[13] J. Leshen, M. Kavai, I. Giannakis, Y. Kaneko, Y. Tokura, S. Mukherjee, W.-C. Lee, and P. Aynajian, Emergent charge order

near the doping-induced Mott-insulating quantum phase transition in $Sr_3Ru_2O_7$, Commun. Phys. **2**, 36 (2019).

[14] P. Massat, J. Wen, J. M. Jiang, A. T. Hristov, Y. Liu, R. W. Smaha, R. S. Feigelson, Y. S. Lee, R. M. Fernandes, and I. R. Fisher, Field-tuned ferroquadrupolar quantum phase transition in the insulator $TmVO_4$, Proc. Natl. Acad. Sci. USA **119**, e2119942119 (2022).

[15] J. M. Moya, A. M. Hallas, V. Loganathan, C.-L. Huang, L. L. Kish, A. A. Aczel, J. Beare, Y. Cai, G. M. Luke, F. Weickert, A. H. Nevidomskyy, C. D. Malliakas, M. G. Kanatzidis, S. Lei, K. Bayliff, and E. Morosan, Field-induced quantum critical point in the itinerant antiferromagnet Ti_3Cu_4, Commun. Phys. **5**, 136 (2022).

[16] V. Zapf, M. Jaime, and C. D. Batista, Bose-Einstein condensation in quantum magnets, Rev. Mod. Phys. **86**, 563 (2014).

[17] P. Pfeuty, The one-dimensional Ising model with a transverse field, Ann. Phys. **57**, 79 (1970).

[18] Z. Wang, T. Lorenz, D. I. Gorbunov, P. T. Cong, Y. Kohama, S. Niesen, O. Breunig, J. Engelmayer, A. Herman, Jianda Wu, K. Kindo, J. Wosnitza, S. Zherlitsyn, and A. Loidl, Quantum criticality of an Ising-like spin-1/2 antiferromagnetic chain in a transverse magnetic field, Phys. Rev. Lett. **120**, 207205 (2018).

[19] Y. Cui, H. Zou, N. Xi, Z. He, Y. X. Yang, L. Shu, G. H. Zhang, Z. Hu, T. Chen, Rong Yu, Jianda Wu, and W. Yu, Quantum criticality of the Ising-like screw chain antiferromagnet $SrCo_2V_2O_8$ in a transverse magnetic field, Phys. Rev. Lett. **123**, 067203 (2019).

[20] F. D. M. Haldane, Spontaneous dimerization in the s = 1/2 Heisenberg antiferromagnetic chain with competing interactions, Phys. Rev. B **25**, 4925(R) (1982).

[21] J. I. Igarashi and T. Tonegawa, Excitation spectrum of a spin-1/2 chain with competing interactions, Phys. Rev. B **40**, 756 (1989).

[22] F. Heidrich-Meisner, I. A. Sergienko, A. E. Feiguin, and E. R. Dagotto, Universal emergence of the one-third plateau in the magnetization process of frustrated quantum spin chains, Phys. Rev. B **75**, 064413 (2007).

[23] E. V. Murashova, Y. A. Velikodnyi, and V. D. Zhuravlev, Crystal structures of double pyrovanadates $CaMgV_2O_7$ and $CaCoV_2O_7$, Russ. J. Inorg. Chem. **38**, 1453 (1993).

[24] S. A. Zvyagin, J. Krzystek, P. H. M. van Loosdrecht, G. Dhalenne, and A. Revcolevschi, High-field ESR study of the dimerized-incommensurate phase transition in the spin-Peierls compound $CuGeO_3$, Physica B: Condens. Matter **346-347**, 1 (2004).

[25] S. Stoll and A. schweiger, Easyspin, a comprehensive software package for spectral simulation and analysis in EPR, J. Magn. Magn. Mater. **178**, 42 (2006).

[26] Y. Skourski, M. D. Kuz'min, K. P. Skokov, A. V. Andreev, and J. Wosnitza, High-field magnetization of Ho_2Fe_{17}, Phys. Rev. B **83**, 214420 (2011).

[27] V. Siruguri, P. Babu, M. Gupta, A. Pimpale, P. Goyal, A high resolution powder diffractometer using focusing optics, Pramana **71**, 1197 (2008).

[28] J. Rodríguez-Carvajal, Recent advances in magnetic structure determination by neutron powder diffraction, Physica B: Condens. Matter **192**, 55 (1993).

[29] See Supplemental Material at http://link.aps.org/supplemental/10.1103/PhysRevResearch.6.L032010 for the crystal structural information, bulk magnetic properties, the bond valence sum analysis, x-ray photoelectron spectroscopy data, discussions on

effective spin-1/2, neutron diffraction and magnetic structure, bulk magnetization experiments on single-crystalline samples, and inelastic neutron scattering (INS) and effective spin-1/2 state.

[30] M. E. Lines, Magnetic properties of $CoCl_2$ and $NiCl_2$, Phys. Rev. **131**, 546 (1963).

[31] H. Shiba, Y. Ueda, K. Okunishi, S. Kimura, and K. Kindo, Exchange interaction via crystal-field excited states and its importance in $CsCoCl_3$, J. Phys. Soc. Jpn. **72**, 2326 (2003).

[32] C. Kim, J. Jeong, G. Lin, P. Park, T. Masuda, S. Asai, S. Itoh, H.-S. Kim, H. Zhou, J. Ma, and J.-G. Park, Antiferromagnetic Kitaev interaction in $J_{eff} = 1/2$ cobalt honeycomb materials $Na_3Co_2SbO_6$ and $Na_2Co_2TeO_6$, J. Phys.: Condens. Matter **34**, 045802 (2022).

[33] J. C. Bonner and M. E. Fisher, Linear magnetic chains with anisotropic coupling, Phys. Rev. **135**, A640 (1964).

[34] A. K. Bera, B. Lake, F. H. L. Essler, L. Vanderstraeten, C. Hubig, U. Schollwöck, A. T. M. N. Islam, A. Schneidewind, and D. L. Quintero-Castro, Spinon confinement in a quasi-one-dimensional anisotropic Heisenberg magnet, Phys. Rev. B **96**, 054423 (2017).

[35] A. Yogi, N. Ahmed, R. Nath, A. A. Tsirlin, S. Kundu, A. V. Mahajan, J. Sichelschmidt, B. Roy, and Y. Furukawa, Antiferromagnetism of $Zn_2VO(PO_4)_2$ and the dilution with Ti^{4+}, Phys. Rev. B **91**, 024413 (2015).

[36] R. Rawl, L. Ge, H. Agrawal, Y. Kamiya, C. R. D. Cruz, N. P. Butch, X. F. Sun, M. Lee, E. S. Choi, J. Oitmaa, C. D. Batista, M. Mourigal, H. D. Zhou, and J. Ma, $Ba_8CoNb_6O_{24}$: A spin-1/2 triangular-lattice Heisenberg antiferromagnet in the two-dimensional limit, Phys. Rev. B **95**, 060412(R) (2017).

[37] M. Kenzelmann, R. Coldea, D. A. Tennant, D. Visser, M. Hofmann, P. Smeibidl, and Z. Tylczynski, Order-to-disorder transition in the XY-like quantum magnet Cs_2CoCl_4 induced by noncommuting applied fields, Phys. Rev. B **65**, 144432 (2002).

[38] G. Novitchi, S. Jiang, S. Shova, F. Rida, I. Hlavička, M. Orlita, W. Wernsdorfer, R. Hamze, C. Martins, N. Suaud, N. Guihéry, A.-L. Barra, and C. Traina, From positive to negative zero-field splitting in a series of strongly magnetically anisotropic mononuclear metal complexes, Inorg. Chem. **56**, 14809 (2017).

[39] A. K. Bera, S. M. Yusuf, A. Kumar, M. Majumder, K. Ghoshray, and L. Keller, Long-range and short-range magnetic correlations, and microscopic origin of net magnetization in the spin-1 trimer chain compound $CaNi_3P_4O_{14}$, Phys. Rev. B **93**, 184409 (2016).

[40] P. Gegenwart, J. Custers, C. Geibel, K. Neumaier, T. Tayama, K. Tenya, O. Trovarelli, and F. Steglich, Magnetic-field induced quantum critical point in $YbRh_2Si_2$, Phys. Rev. Lett. **89**, 056402 (2002).

[41] M. Garst and A. Rosch, Sign change of the Grüneisen parameter and magnetocaloric effect near quantum critical points, Phys. Rev. B **72**, 205129 (2005).

[42] L. S. Wu, S. E. Nikitin, Z. Wang, W. Zhu, C. D. Batista, A. M. Tsvelik, A. M. Samarakoon, D. A. Tennant, M. Brando, L. Vasylechko, M. Frontzek, A. T. Savici, G. Sala, G. Ehlers, A. D. Christianson, M. D. Lumsden, and A. Podlesnyak, Tomonaga–Luttinger liquid behavior and spinon confinement in $YbAlO_3$, Nat. Commun. **10**, 698 (2019).

[43] A. W. Kinross, M. Fu, T. J. Munsie, H. A. Dabkowska, G. M. Luke, S. Sachdev, and T. Imai, Evolution of quantum fluctuations near the quantum critical point of the transverse field ising chain system $CoNb_2O_6$, Phys. Rev. X **4**, 031008 (2014).

[44] Y. Fan, J. Yang, W. Yu, J. Wu, and R. Yu, Phase diagram and quantum criticality of Heisenberg spin chains with Ising anisotropic interchain couplings, Phys. Rev. Res. **2**, 013345 (2020).